Polarized Neutron Scattering and Polarization Analysis

W. Schweika

This document has been published in

Manuel Angst, Thomas Brückel, Dieter Richter, Reiner Zorn (Eds.):
Scattering Methods for Condensed Matter Research: Towards Novel Applications at Future Sources
Lecture Notes of the 43rd IFF Spring School 2012
Schriften des Forschungszentrums Jülich / Reihe Schlüsseltechnologien / Key Technologies, Vol. 33
JCNS, PGI, ICS, IAS
Forschungszentrum Jülich GmbH, JCNS, PGI, ICS, IAS, 2012
ISBN: 978-3-89336-759-7

C 6 Polarized Neutron Scattering and Polarization Analysis [1]

W. Schweika

Jülich Centre for Neutron Science

Forschungszentrum Jülich GmbH

Contents

[1] Lecture Notes of the 43^{rd} IFF Spring School "Scattering Methods for Condensed Matter Research: Towards Novel Applications at Future Sources" (Forschungszentrum Jülich, 2012).

1 Introduction

Among the properties that make the neutron a unique and valuable probe for condensed matter research, its spin and magnetic moment is of particular importance in the scattering process. There are two aspects to consider, firstly, the strong nuclear interaction of the neutron with an nucleus depends on the either parallel or antiparallel alignment of the spins of neutron and nucleus, and secondly, the neutron's magnetic moment interacts with the unfilled electron shells of atoms or ions in magnetic scattering. The scattering process will also have an impact on the spin state of the neutron probe. Hence, one may expect that controlling the neutron spin in a scattering experiment will provide further valuable information, which leads us to the subject of this lecture: polarized neutron scattering and polarization analysis. Indeed, it is possible by working with polarized neutron and polarization analysis to separate scattering terms with respect to their different structural or magnetic origins, and moreover, to uncover scattering contributions that remain hidden in usual unpolarized scattering experiments.

2 Neutron spins in magnetic fields

The neutron has a spin $S = \pm 1/2$ with angular momentum $\mathbf{L} = \hbar\mathbf{S}$. The magnetic moment of the neutron results from the spins of the individual quarks and their orbital motions, and the relation between spin and magnetic moment is given by the neutron g-factor, $g_n = -3.8260837(18)$, in units of the nuclear magneton $\mu_N = \frac{e\hbar}{2m_p} = 5.05078324(13) \cdot 10^{-27}\mathrm{JT}^{-1}$

$$\mu_n = g_n S \mu_N \simeq \mp 1.913 \mu_N = \pm \gamma_n \mu_N,$$

where $\gamma_n = -g_n S$ is the gyromagnetic factor of the neutron (see Refs. [1, 2]) . Because of the small ratio $\mu_n/\mu_B = m_e/m_p$, the neutron magnetic moment μ_n is small compared to the magnetic moment of the electron $\mu_e = g_e S \mu_B \approx 1\mu_B$, with the Bohr magneton $\mu_B = \frac{e\hbar}{2m_e}$ and the Lande-factor $g_e = 2(1 + \alpha/2\pi - 0.328\alpha^2/\pi^2) \approx 2$ (see Refs. [3, 4]), α is the fine structure constant. A peculiarity to note is that different to the electron and proton, the neutron magnetic moment is aligned opposite to its spin.

2.1 Interaction of neutrons with magnetic fields

The dipolar interaction potential of a neutron with the magnetic field is given by $V_M = -\boldsymbol{\mu_n} \cdot \mathbf{B}$, where $\mathbf{B}$ is the magnetic induction. For neutrons passing from zero-field into a magnetic field the potential energy changes by the Zeeman term $\pm\mu_n \mathrm{B}$ depending on the relative orientation of the magnetic moment. The according change in kinetic energy to conserve the total energy is small, $0.06\,\mu\mathrm{eV/T}$, which in experimental practice is of relevance only in rare cases [5].

Larmor precession

The characteristic motion of the neutron magnetic moment in a magnetic field is Larmor precession, which for simplicity can be considered in a classical treatment. In fact, even the quantum mechanical treatment, which introduces Pauli spin matrices $\hat{\boldsymbol{\sigma}}$ into the Schrödinger equation, is effectively a classical treatment considering the origin of these matrices. Originally[6], they result from the problem of mapping three dimensions onto two by introducing a complex component describing the classical problem of a spinning top.[7]

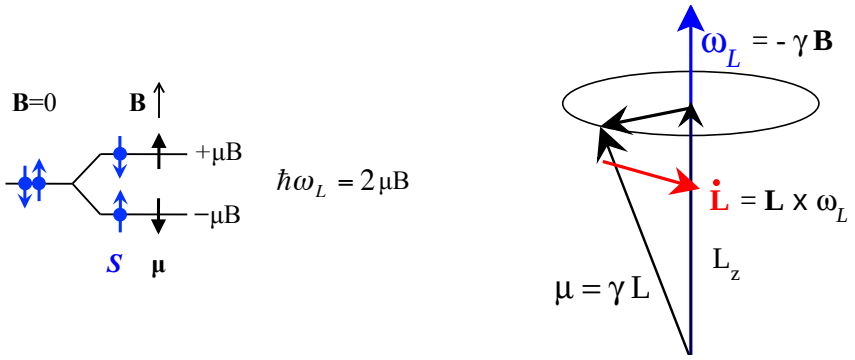

Fig. 1: *Larmor precession: the motion of the neutron in a constant magnetic field conserves energy and angular momentum.*

The magnetic interaction tends to align the neutron moment with the magnetic induction in order to minimize the interaction energy. The magnetic moment is related to the angular momentum as $\boldsymbol{\mu} = \gamma \mathbf{L}$, where γ is the gyromagnetic ratio. Therefore, there is a torque $\boldsymbol{\mu} \times \mathbf{B} = \dot{\mathbf{L}}$ equal to the time derivative of the angular momentum, which leads to the Bloch equation of motion:

$$\dot{\boldsymbol{\mu}} = \gamma \, \boldsymbol{\mu} \times \mathbf{B}. \tag{1}$$

The gyromagnetic *ratio* for the neutron, not to be confused with the gyromagnetic factor, is given by $\gamma = 2\gamma_n \mu_N / \hbar = -1.83 \cdot 10^8 \, \mathrm{s}^{-1}\mathrm{T}^{-1}$ or, in cgs units, $\gamma/2\pi = -2916 \, \mathrm{Hz/Oe}$. Because of the cross product, the time derivative of the magnetic moment is always perpendicular to the moment itself. Therefore, the resulting motion is a precession, where the angular momentum, the component L_z along the field, and the energy are constants of the motion, see Fig.1. The precession frequency is the *Larmor frequency* $\omega_L = -\gamma B$, and $\hbar\omega = 2\mu B$, the Zeeman splitting energy.
Next we consider the many particle ensemble of neutrons in a neutron beam. Polarization of a neutron beam is defined by the normalized average over the neutron spins.

$$\mathbf{P} = 2\langle \mathbf{S} \rangle \tag{2}$$

In an applied field the individual neutrons split in spin up $n_\uparrow$ and and spin down states $n_\downarrow$. Since polarization will be measured with respect to a magnetic field defining a quantization axis, any device for polarization analysis will take the projection of the spins in up- and down state states,

$$\mathrm{P} = \frac{n_\uparrow - n_\downarrow}{n_\uparrow + n_\downarrow}. \tag{3}$$

Motion in time dependent fields

The polarization will behave like the individual neutron spin in a constant magnetic field and will be a constant of motion. However, if we consider time-dependent fields, the finite velocity distribution in a neutron beam will result in a different time dependence. Hence dephasing of neutrons spins and degrading of the polarization are possible experimental effects and have to be taken into account.
Thermal neutrons move with a speed of thousands of meters per second. When passing through spatially varying magnetic fields, the neutrons experience time-dependent field changes in their

reference system. Replacing the constant $\mathbf{B}$ by $\mathbf{B}(t)$, the differential equation Eq. (1) can be used to calculate numerically the effect of all relevant field variations in an experimental set-up. Usually, it is possible to work within two simple limiting cases of either **(i) slow adiabatic field variation**, in which the non-precessing spin component parallel to the field smoothly follows the field direction, or of **(ii) sudden field reversal**, in which the non-precessing spin component has no time to reorient itself, when traversing abruptly from a parallel to anti-parallel field or vice versa. Slow field variation means that the field $\mathbf{B}$ changes or rotates in the coordinate system of the neutron with a frequency that is small compared to the Larmor frequency, see Fig. 1.

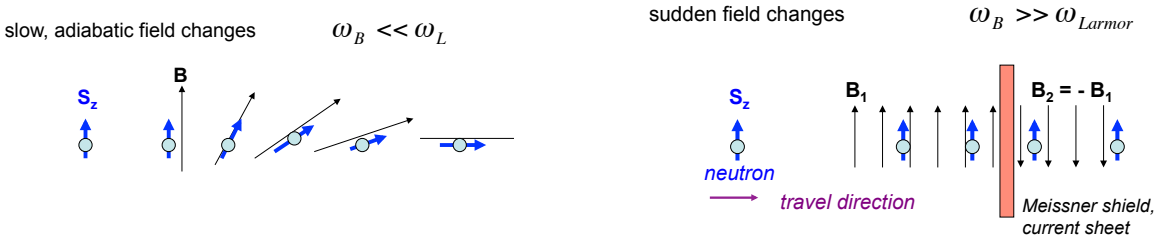

Fig. 2: *Neutron polarization can be best preserved in the asymptotic cases of either slowly or suddenly varying fields. The second case is used in a cryoflipper to reverse the polarization with respect to the external field.*

2.2 Experimental devices

Polarizer and polarization analyzer

The most common methods to polarize neutrons are (i) using the total reflection from magnetic multi-layers, (ii) using Bragg reflection of polarizing single crystals (typically Heusler crystals) and (iii) polarized He-3 filters, in which for anti-parallel spins the (n,^{3}He)-compound has a large absorption cross-section while all neutrons with parallel spins may pass the filter cell. The first two methods use an interference effect of nuclear and magnetic scattering amplitudes having the same absolute value.

(i) Polarizing total reflecting supermirrors are an easy experimental tool to obtain a broad wavelength band of cold polarized neutrons. The angle of total reflection for a single ferromagnetic (FM) layer is given by

$$\Theta_c^{\pm} = \lambda\sqrt{n(b-p)/\pi}. \tag{4}$$

Here n denotes the particle density and b and p the nuclear and magnetic scattering lengths, respectively. However, the critical angle can be further increased by artificial multi-layers (supermirrors) of alternating FM and non-magnetic layers of varying thickness [8], see Fig. 3. The λ dependence of the total reflectivity makes this type of polarizer less favorable for thermal neutrons of shorter wave length as it reduces the accepted divergence of the beam.

(ii) Bragg reflection by Heusler crystals is alternatively used to polarize thermal neutrons. Cu_2MnAl is a Heusler alloy, its (111) Bragg reflection gives 95 % polarization. However, the reflectivity of such crystals is low compared to usual non-polarizing monochromators and a saturating field is required over the entire monochromator, which makes it technically more complicated to combine with focusing though this is feasible.

(iii) He-3 filter cells, see Fig. 4, are of growing importance for polarizing neutrons, particularly for the more challenging case of thermal neutrons, although such cells are technically rather demanding and still under development. In case of spin-exchange optical pumping (SEOP) the spin polarization of ^{3}He gas is achieved in several steps. The cell is filled with additional Rb, K and N_2 vapor. Rb electrons are polarized with a a circular polarized laser, by collisions the spin is exchanged with K, which most efficiently exchanges spin with ^{3}He. Since polarization results from absorption, such a device does not interfere with the beam divergence. One may note that requirements for field homogeneity are very high and it is a kind of art and glass alchemy to make cells with small depolarization all determining the lifetime of He-3 polarization. The neutron polarization P raises with increasing He-3 cell size or pressure, while the transmission T decreases. The optimum in efficiency is usually chosen by the maximum of a quality factor P^2T.

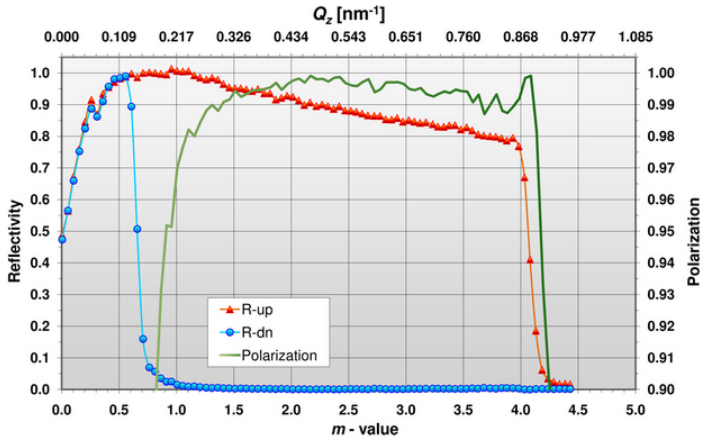

Fig. 3: *Spin dependent reflectivity and polarisation of a Fe/Si polarizing supermirror. The degree of polarization is high, note the expanded scale .* m=1 *($Q = 0.0217$Å^{-1}) corresponds to the total reflectivity of natural Ni. (from [9])*

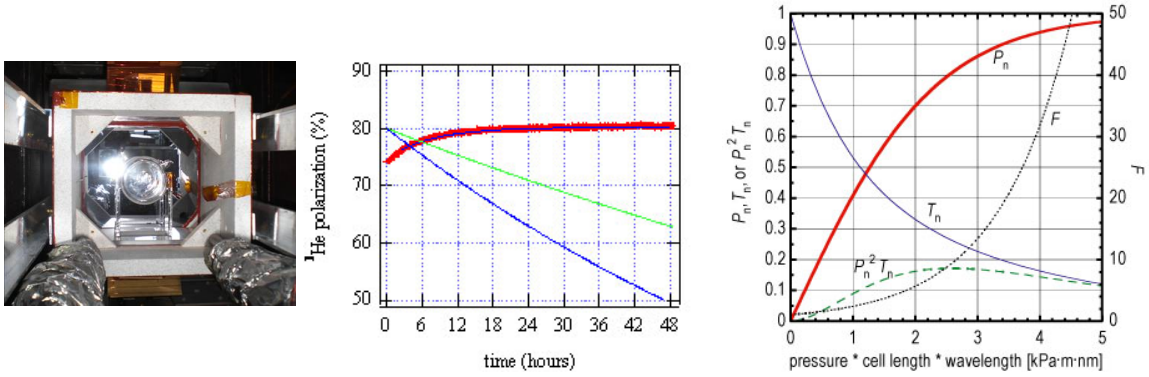

Fig. 4: *In-situ polarization of a SEOP He-3 cell and measured polarization of neutron beam in transmission. (from Babcock et al.[10])*

Guide-fields

A magnetic *guide field* is used to maintain the direction of the spin and the polarization of the neutron beam. The guide field preserves the quantization axis to which the neutron moments have align either parallel or anti-parallel. Typical guide fields in the order of 10 G are strong compared to earth field and other possible stray fields and usually sufficient to prevent depolarization along the beam path. Such guide fields are usually also too weak to have any significant impact on the sample magnetization.
Depolarization effects may for an inhomogeneous distribution of field directions over neutron beam cross-section, which is typically a few cm^2. This can easily occur if ferromagnetic material is used close to the beam or if the sample itself is ferromagnetic. A neutron beam passing through a ferromagnet is usually completely depolarized by differently oriented ferromagnetic domains in the beam path, unless a saturating magnetic field is used to align the domains. Depolarization will depend also on the path length through the sample, therefore, usually such effects are negligible in *neutron reflectometry* of thin ferromagnetic films.

Flipper

The purpose of a **π-flipper** is to reverse the polarization and to detect whether the sample causes spin-flip scattering.
When applying a magnetic field perpendicular to the polarized neutron beam, the polarization immediately starts its Larmor precession. A flipper that reverses the neutron polarization with respect to the guide field has to induce a well-defined field pulse so that the polarization precesses by an angle π. For this purpose one can use the homogeneous field of a $Mezei$ flipper, a long rectangular coil, see Fig. 5. Neutrons see a sudden field change when they enter and exit the coil, in between they precess around the perpendicular flipping field, whose magnitude is tuned with respect to the time of flight that the neutrons spend inside the coil. Thus, for a π flip in coil of thickness d, the time-of-flight $t = d\lambda\frac{m}{h} = \pi/\omega = -\pi/\gamma B$, (for example λ=4Å, B=17G, d=1cm). Just to mention, other types of flippers exist like radio frequency (RF) flipper (setup Moon, Riste Koehler, Fig. 8 and cryoflipper (Fig.2 and CryoPad Fig.10).

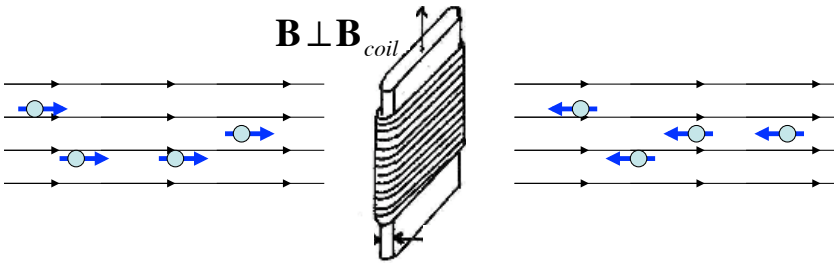

Fig. 5: *Principle of a neutron π-spin flipper. The neutrons perform a Larmor-precession of* 180^o *inside a long rectangular coil. The field $\boldsymbol{B}$ is perpendicular to spin orientation and adjusted to the speed of the neutrons.*

The purpose of a **π/2-flipper** is to set the polarization in precession mode by turning the polarization perpendicular to the guide field. A precessing polarization is used for instance in high resolution *Neutron Spin Echo spectroscopy* and for *Larmor diffraction*, see below. Both methods use the property of the neutron spin as an internal clock independent of the scattering process itself and achieve highest resolution.

Precessing polarization can also be used for analyzing polarization dependent scattering. A polarization analyzer accepts neutrons with spins aligned with respect to the magnetic guide field axis. If prior to the scattering process the neutron polarization is precessing with a known phase and if then finally we detect a neutron polarization along the guide field, we can conclude that scattering has caused the observed rotation of polarization. This method can be used for *neutron polarimetry* or *spherical polarization analysis*.

XYZ-coils

In order to align the polarization to any desired direction at the sample position, there is in the simplest version a set-up of three orthogonal pairs of so-called xyz-coils. Fig. 6 illustrates the field setting along x-direction. With such a device one can probe the direction of magnetic moments in the sample. One can see that the z-coil has been used to compensate the guide field at the sample position, and that the x-coils produce a field of a few Gauss. The field needs to be sufficiently strong so that the neutron polarization can follow the smooth variation of the field direction adiabatically, finally turning back into the z-direction of the guide field outside the xyz-coils.

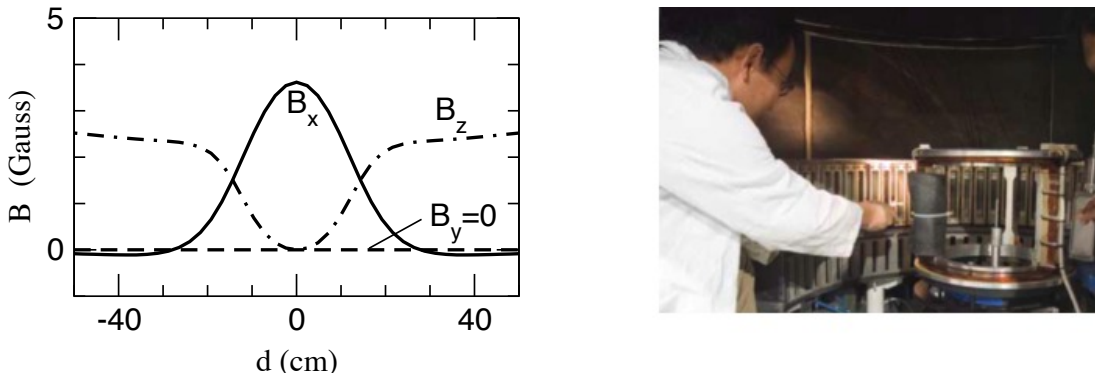

Fig. 6: *(left) Magnetic field setting in a xyz-coil system for an adiabatic nutation of the polarization of cold neutrons in horizontal x-direction at the sample turning to a vertical (guide) field B_z at further distance from the sample. (right) A photo of the xyz-coil system in the DNS instrument at the FRM-2.*

2.3 Polarized neutron instrumentation

The spin of the neutron and its Larmor precession in a magnetic field is an individual property of each neutron that can also used to measure indirectly the momentum or energy transfer in a scattering process, and with extremely high resolution. The ideas of the two most interesting applications of neutron precession spin-echo spectroscopy and Larmor diffraction will be discussed next.

Of course, the main objective of polarized neutron work is determine the polarization dependence of scattering. The selected examples below are important but cannot give an exhaustive overview on the suite of polarized neutron instrumentation, which is of growing diversity.

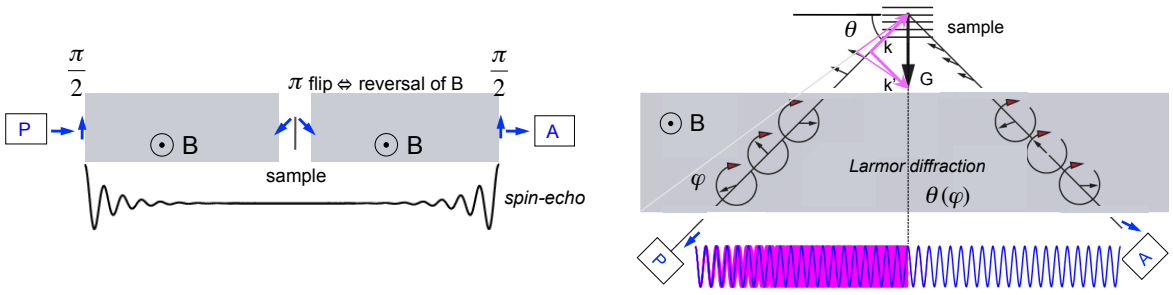

Fig. 7: *Precession in spin-echo spectroscopy (*left*) and Larmor diffraction (*right*, adapted from [13]).*

Neutron precession techniques

The idea of **neutron spin echo spectroscopy** is to use the individual spin precession of the neutrons to monitor possible small energy transfers of approximately 1μeV upon scattering. The incident beam is polarized first parallel to the field, then set into precession mode by a $\pi/2$ flipper and along the path through the precession coil, the total precession angle of the neutron is increases proportional to the time in the coil. Because $t \propto \lambda$, soon neutron spins are out of phase and the polarization vanishes to zero, which however can be fully recovered. Therefore, in the simplest case of elastic scattering, an equivalent field of opposite direction in the secondary flight path will turn the precession angles of all neutrons backwards and a spin echo - after another $\pi/2$ flip - can be detected by the final polarization analyzer. Energy exchange with the sample changes the average neutron speed and to recover the full spin echo the field integral has to be varied and adjusted. For a more precise understanding of the general inelastic case, we note that this is a special diffraction experiment, in which the energy transfer integral of the scattering law $S(\mathbf{Q},\omega)$ is weighted with $\mathbf{P}$ $(= P_z)$:

$$I \propto \int d\omega\, P_{(z)} S(\mathbf{Q},\omega) = \frac{1}{2}(S(Q) + \int d\omega\, \cos(\phi) S(\mathbf{Q},\omega)),$$

where $S(\mathbf{Q})$ gives the average from the unpolarized case. With $\phi = \omega t = \text{const} \cdot \omega \int ds\, B$ and identifying $\text{const} \int ds\, B = t$ as a Fourier time, one obtains

$$I \propto \frac{1}{2}(S(Q) + S(Q,t)).$$

In **Larmor diffraction**, all of the neutrons, which make the same Bragg reflection undergo the same number of precessions. Hence, the full neutron polarization is preserved and can be measured; there is no dephasing because of wavelength spread, beam divergence and mosaic of the sample. The total precession angle ϕ is proportional to the time t in the magnetic field region, and $t = s/v =$ is constant for a given Bragg reflection, since $s(\theta) \propto k$ and $v \propto k$, any spread in k distribution is compensated. Furthermore, the sum of incoming and outgoing flight path through the precessing region remains practically constant for a mosaic of the crystal, *i.e.* small tilts of the Bragg planes. Moreover, a combination of Larmor diffraction with the spin-echo principle, by introducing a π-flip near to the sample, allows to measure the mosaic by a loss in polarization.[11] Absolute d-spacings have been measured with $7 \cdot 10^{-5}$ Å accuracy.[12]

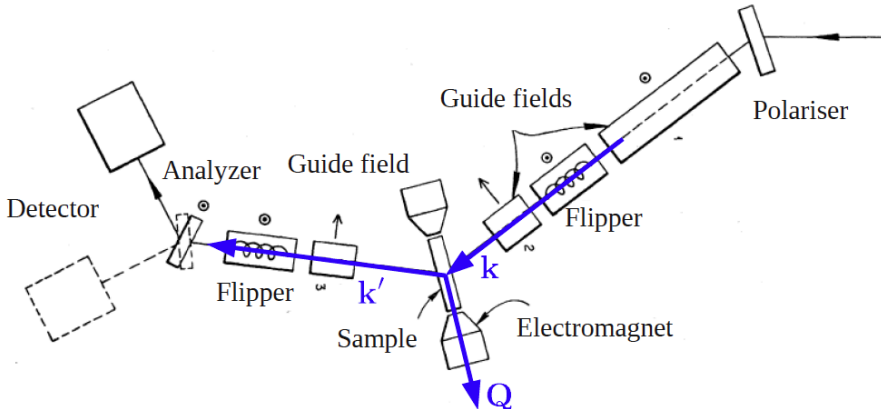

Fig. 8: *Setup for polarization analysis on a triple axis instrument by Moon* et al.*(1969)[14], see also text.*

Uniaxial polarization analysis on 2- and 3-axis instruments

Uniaxial polarization analysis means that not the full final polarization but only the projection of the final polarization with respect to an applied field is measured. There are a large number of triple axis instruments (TAS), which offer in various technical realizations the principle of uniaxial polarization analysis. ln the original setup by Moon, Riste and Koehler[14] at the Oak Ridge reactor (HFIR), see Fig.15, Co-Fe crystals mounted in the gap of permanent magnets are used on the first and third axis for the production of the polarized monochromized beam and for analysis of the scattered neutrons in energy and spin state. At the second axis with the sample an electromagnet can be turned to set the field either vertically or horizontally. Radio-frequency coils are used as flipping devices.

XYZ polarization analysis on time-of-flight multi detector instruments

The diffuse neutron scattering spectrometer DNS at the FRM2 in Munich is equipped with polarization analysis and is particularly devoted to elastic and inelastic diffuse scattering that may arise from spin correlations and magnetic disorder and ordering in materials. A layout of the instrument is shown in Fig. 9. DNS is a time-of-flight instrument[15] with a multi-detector system similar to the D7 instrument at the ILL [16, 17]. The monochromatic incident beam is polarized with a focusing supermirror bender, xyz-field coils allow for a change of the polarization at the sample, and the polarization analysis is performed with supermirror analyzers in focusing arrangement in front of each detector.

Zero-field spherical polarization analysis - CryoPad

The CryoPad is a portable, cryogenic device developed at the ILL by Tasset and LeLievre-Berna, which avoids any magnetic field and precession at the sample and achieves full and accurate control of change and rotation of incident to final polarization. As scheme and a set-up on the POLI-HEIDI instrument at FRM-2 is depicted in Fig.10.

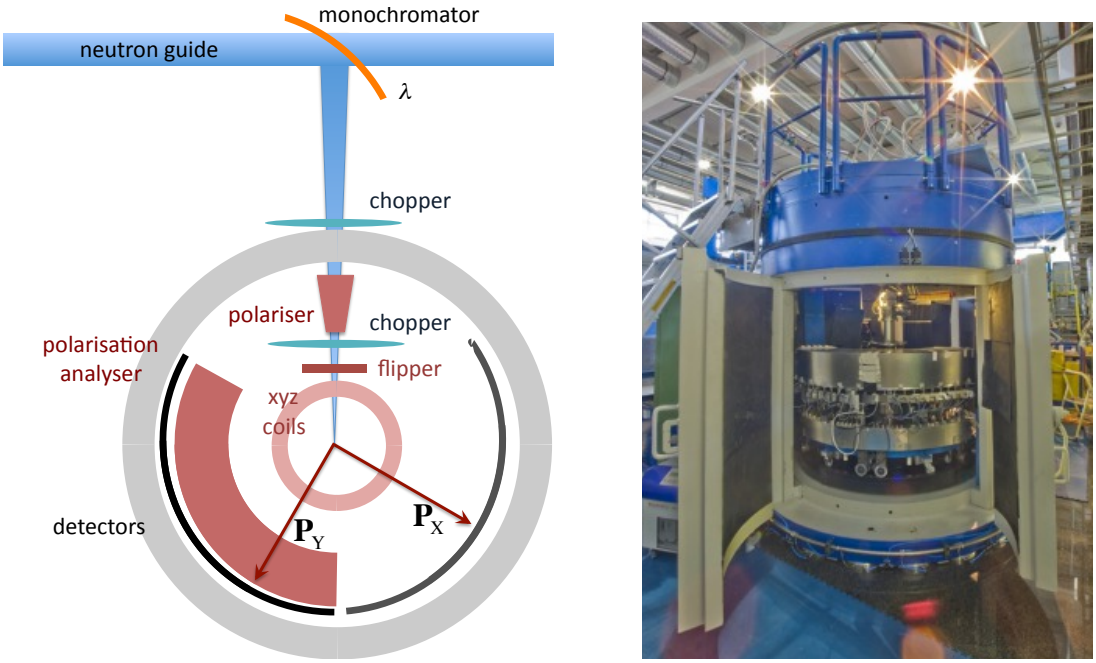

Fig. 9: *Polarization analysis on a time-of-flight multi-detector instrument, the DNS instrument at FRM-2, see Ref.[30] for the specific setting of polarization.*

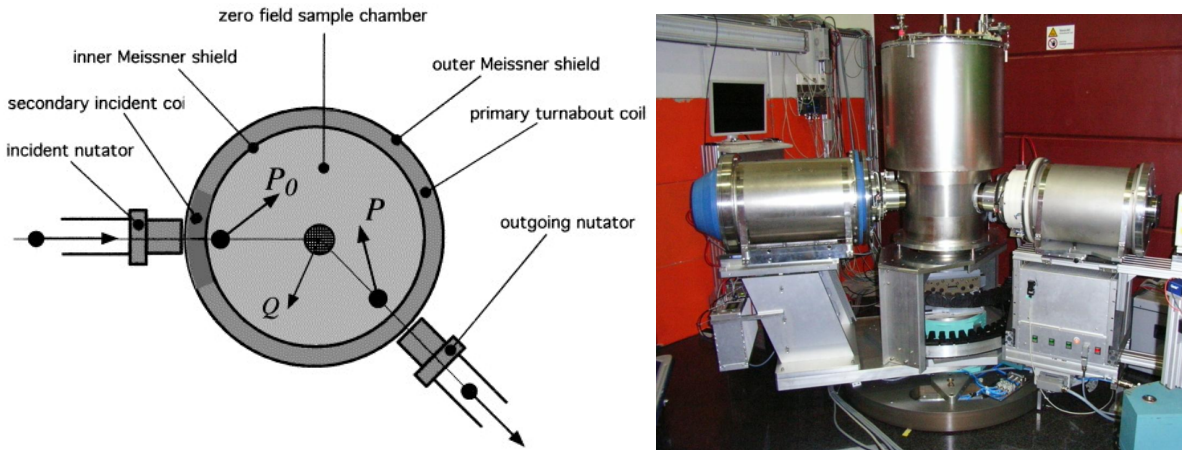

Fig. 10: *CryoPad (scheme)[18] and set-up at POLI-HEIDI (FRM-2). The zero-field around the sample avoids a precession of the beam polarization and allows to measure changes in magnitude and direction of* $\mathbf{P}$ *by scattering.*

3 Scattering and polarization

3.1 Interaction of neutrons with matter

The neutron scattering amplitude $F_{\mathbf{Q}}$ is determined by the transition matrix elements for a given scattering potential $V_{\mathbf{Q}}$

$$F_{\mathbf{Q}} = \langle \mathbf{k}'\mathbf{S}'|V_{\mathbf{Q}}|\mathbf{k}\mathbf{S}\rangle \tag{5}$$

resulting in a scattering cross section that in general depends on the scattering vector $\mathbf{k}-\mathbf{k}' = \mathbf{Q}$ and also on the energy transfer, which for simplicity will not be included in the notation:

$$\frac{d\sigma}{d\Omega} = \left(\frac{m_n}{2\pi\hbar^2}\right)^2 |F|^2 \tag{6}$$

The **nuclear interaction** operator $\hat{V} = (2\pi\hbar^2/m_n)\hat{b}$ can be described by a point-like and isotope-specific Fermi potential. For nuclei with zero spin (*e.g.* ^{12}C, ^{16}O ..., and typically *"gg"* isotopes with even number of protons and neutrons) the scattering length operator $\hat{b}$ is a scalar and the scattering will be independent of the neutron spin orientation.
The interaction is spin-dependent if the scattering nuclei have a non-zero spin $\mathbf{I}$ and the scattering lengths differ for parallel and antiparallel alignment of $\mathbf{I}$ and $\mathbf{S}$, which can be written as the sum of an average and coherent part A and a fluctuating spin-dependent part

$$\hat{\mathbf{b}} = A + B\ \hat{\boldsymbol{\sigma}} \cdot \hat{\mathbf{I}} \tag{7}$$

where $\hat{\boldsymbol{\sigma}}$ is the Pauli spin operator given by Pauli spin matrices $\hat{\sigma}_{\mathrm{x}} = \begin{pmatrix} 0 & 1 \\ 1 & 0 \end{pmatrix}$, $\hat{\sigma}_y = \begin{pmatrix} 0 & -\mathrm{i} \\ \mathrm{i} & 0 \end{pmatrix}$, $\hat{\sigma}_z = \begin{pmatrix} 1 & 0 \\ 0 & -1 \end{pmatrix}$. Defining a quantization axis z for the neutron polarization $\mathbf{P} = 2\langle\hat{\mathbf{S}}\rangle = \langle\,\hat{\boldsymbol{\sigma}}\rangle$, with spin-up states $|+\rangle = \binom{1}{0}$ and spin-down states $|-\rangle = \binom{0}{1}$ we obtain the transition matrix elements

$$\langle +|\,\hat{\boldsymbol{\sigma}} \cdot \hat{\mathbf{I}}|+\rangle = I_z, \tag{8}$$

$$\langle -|\,\hat{\boldsymbol{\sigma}} \cdot \hat{\mathbf{I}}|+\rangle = I_x + \mathrm{i}I_y, \tag{9}$$

for non-spinflip and spinflip scattering amplitude, respectively. Therefore, two thirds of the spin-incoherent scattering is spinflip scattering. The final polarisation is given by $\mathbf{P}' = -\frac{1}{3}\mathbf{P}$. There is a change in sign and a reduction in magnitude, but no inclination towards $\mathbf{P}$. We may note that in contrast to the dipolar magnetic interaction, as discussed below, the obtained result is independent of the direction of $\mathbf{P}$ with respect to $\mathbf{Q}$.

In summary, we can distinguish three contributions to the nuclear scattering $|N_{\mathbf{Q}}|^2$ arising from the total nuclear scattering amplitude $N_{\mathbf{Q}} = \sum_j b_j e^{i\mathbf{Q}\cdot\mathbf{R}_j}$, the average coherent scattering, the isotopic, non-spin dependent part of the incoherent scattering, and the spin-incoherent scattering

$$\frac{d\sigma}{d\Omega}^N_{\mathbf{Q}} = |N_{\mathbf{Q}}|^2 = \frac{d\sigma}{d\Omega}^N_{\mathbf{Q},coh} + \frac{d\sigma}{d\Omega}^N_{isotop-inc} + \frac{d\sigma}{d\Omega}^N_{spin-inc}. \tag{10}$$

In absence of magnetic scattering, the sum of the coherent and isotopic incoherent nuclear scattering can be separated from the spin-incoherent scattering by measuring spin-flip and non-spin-flip scattering.

$$\frac{d\sigma}{d\Omega}^N_{\mathbf{Q},coh} + \frac{d\sigma}{d\Omega}^N_{isotop-inc} = \frac{d\sigma}{d\Omega}^{NSF} - \frac{1}{2}\frac{d\sigma}{d\Omega}^{SF} \tag{11}$$

$$\frac{d\sigma}{d\Omega}_{spin-inc} = \frac{3}{2}\frac{d\sigma}{d\Omega}^{SF} \tag{12}$$

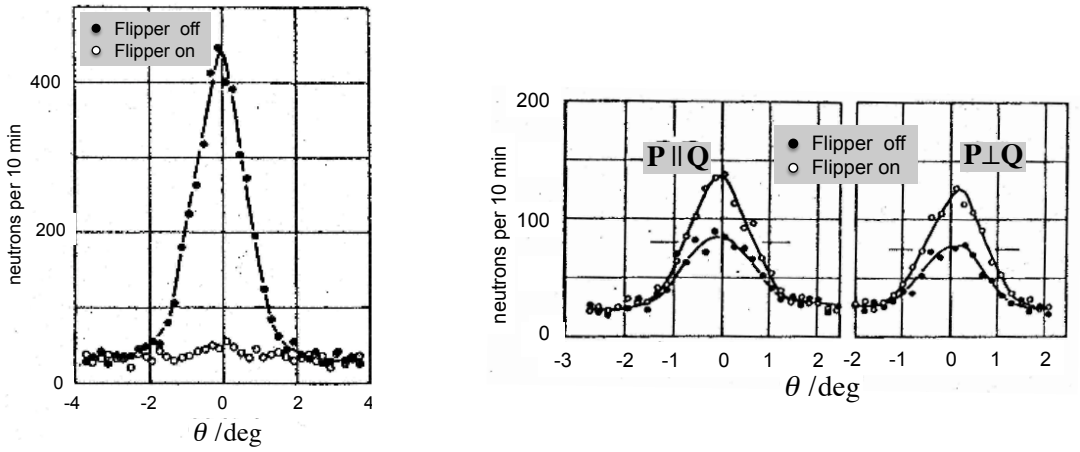

Fig. 11: Left*: Nuclear isotopic incoherent scattering from nickel obtained by rocking the analyzer crystal through the elastic position, which is essentially all non-spin-flip scattering.*
Right: *Nuclear spin-incoherent scattering from vanadium show 2/3 and 1/3 contributions in the spin-flip and non-spin-flip channel respectively. There is no dependence on the direction of* $\mathbf{P}$ *relative to* $\mathbf{Q}$ *for all nuclear scattering (from Ref.[14]).*

Applications to local order in disordered hydrogeneous materials

Typical soft matter samples contain hydrogen which causes a huge spin-incoherent background ($\sigma_{inc}(H) = 80\,\mathrm{b}$) in the wide-angle scattering that contains information about local correlations ($\sigma_{coh}(H) = 1.76\,\mathrm{b}$). Here, a precise determination of coherent scattering can be achieved by measuring spin-flip and non-spin-flip scattering. It is particularly valuable to combine this further with the method of contrast variation using H and D isotopes, having rather distinct scattering lengths, $b_{coh}(H) = -0.374 \cdot 10^{-12}\mathrm{cm}$ and $b_{coh}(D) = 0.667 \cdot 10^{-12}\mathrm{cm}$. Fig. 12 shows the separated coherent scattering of a polymer glass. Such results provide most useful information about local order that can be compared to molecular dynamics simulations of theoretical polymer models [20].

Applications to dynamics in liquids

Since in a liquid all atoms are moving around, the scattering is not elastic as in the case of Bragg peaks from a solid, single crystal. Diffraction - the energy integrated scattering - provides us with structural properties from a snap-shot of typical atomic configurations. Since neutron energies are comparable to thermal energies involved in atomic motions, it is relatively simple to achieve an adequate energy resolution to study the dynamics for instance in liquids. Therefore, a typical instrument set-up uses the time-of-flight technique: the monochromatic beam is pulsed by a mechanical chopper and the measured *time-of-flight* of the neutrons can be related to an energy transfer in the sample. Note, the separation by polarization analysis in *coherent* scattering and spin-*incoherent* scattering distinguishes *pair-correlations* from *single particle correlations*, respectively. The following example of liquid sodium [21] demonstrates in a very instructive way the complementary information that can be obtained. From simple liquid models one expects that the incoherent scattering has a Lorentzian shape in energy at constant Q, related to exponential relaxations in time, with a width that for the macroscopic limit, $Q \to 0$, is related to the macroscopic diffusion constant. On the other hand, the coherent scattering is

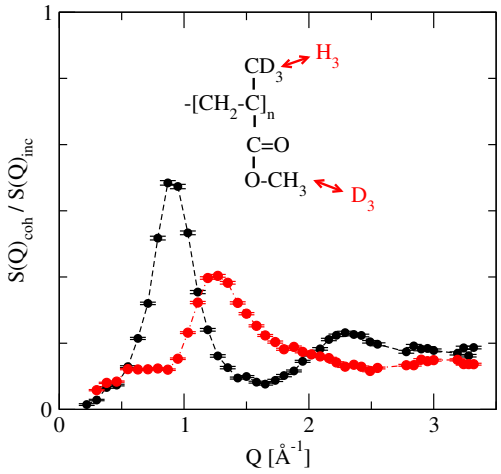

Fig. 12: *Neutron polarisation analysis separates coherent scattering from spin-incoherent scattering, which is typically a disturbing large background in materials that contain hydrogen, while here it provides a precise intrinsic calibration. In addition, H/D contrast varies the coherent scattering of a polymer glass PMMA.[20]*

rather different and exhibits a pronounced peak related to typical nearest neighbor distances reflecting precursors of Bragg peaks and crystalline order, see Fig. 13.

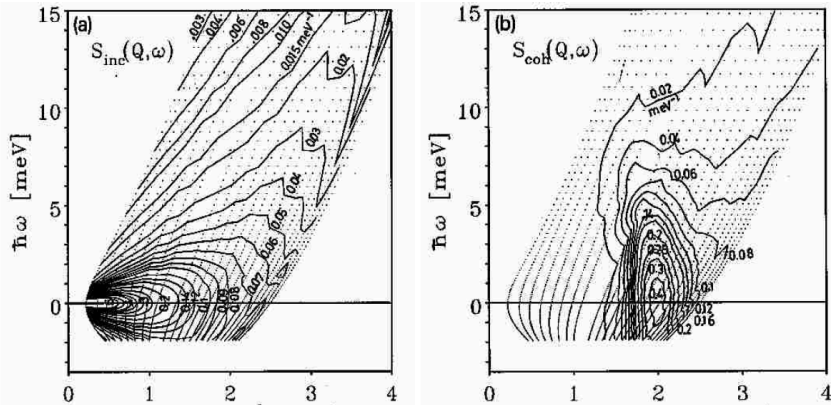

Fig. 13: *Contour plot of a) spin-incoherent and b) coherent scattering of liquid sodium at T=840 K separated by polarization analyis (taken from Ref.[21]). The dotted mesh corresponds to the coordinates of time-of-flight and scattering angles.*

The **magnetic interaction potential** is given by

$$V_m = -(\gamma_n r_0/2)\hat{\boldsymbol{\sigma}} \cdot \hat{\mathbf{M}}_{\mathbf{Q}}^{\perp}, \tag{13}$$

where $\hat{\mathbf{M}}_{\mathbf{Q}}^{\perp}$ is the operator of the magnetic interaction vector,

$$\mathbf{M}_{\mathbf{Q}}^{\perp} = \mathbf{e}_{\mathbf{Q}} \times \mathbf{M}_{\mathbf{Q}} \times \mathbf{e}_{\mathbf{Q}} \tag{14}$$

which is reduced to only the perpendicular components of $\mathbf{M}_{\mathbf{Q}}$ with respect to $\mathbf{Q}$. $\mathbf{M}_{\mathbf{Q}}$ represents the total Fourier transform of the spin and orbital contribution to the magnetization density. The reason for the anisotropy of the interaction is due to the dipolar interaction of the neutron spin with the magnetic moments [19], which it is illustrated in Fig. 14. The components of a magnetic dipole field parallel to the scattering vector $\mathbf{Q}$ cancel out. Therefore, in contrast to the spin-incoherent scattering, magnetic scattering is anisotropic with respect to $\mathbf{Q}$ and only $\mathbf{M}_{\mathbf{Q}}^{\perp}$, the components perpendicular to $\mathbf{Q}$ can be observed.

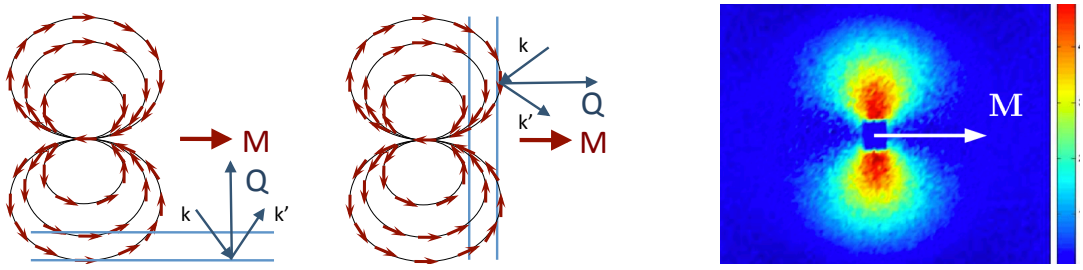

Fig. 14: *Illustration why only* $\mathbf{M}_{\mathbf{Q}}^{\perp}$ *is measured. For* $\mathbf{M} \perp \mathbf{Q}$*, magnetic dipole field amplitudes show constructive interference, for* $\mathbf{M} \parallel \mathbf{Q}$ *destructive interference.* Right: *Polarized small angle scattering probing the magnetization of iron oxide nanoparticles.[22]*

In analogy to the spin-dependent nuclear interaction, we obtain the transition matrix elements for the magnetic interaction, choosing z-polarization and x parallel to $\mathbf{Q}$, $\mathbf{M}_{x,\mathbf{Q}}^{\perp} = 0$, and

$$\langle + |\, \hat{\boldsymbol{\sigma}} \cdot \hat{\mathbf{M}}_{\mathbf{Q}}^{\perp} | + \rangle \;=\; \mathbf{M}_{z,\mathbf{Q}}^{\perp}, \tag{15}$$

$$\langle - |\, \hat{\boldsymbol{\sigma}} \cdot \hat{\mathbf{M}}_{\mathbf{Q}}^{\perp} | + \rangle \;=\; \mathrm{i}\mathbf{M}_{y,\mathbf{Q}}^{\perp}. \tag{16}$$

Hence, as illustrated in Fig. 15, the component of $\mathbf{P}$ parallel to $\mathbf{M}_{\mathbf{Q}}^{\perp}$ remains unchanged, while

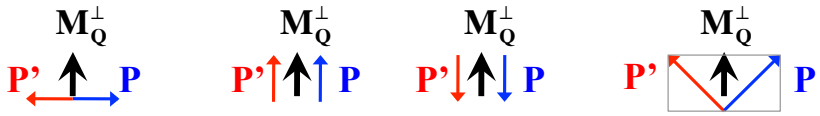

Fig. 15: *Change of initial polarization* $\mathbf{P}$ *to final polarization* $\mathbf{P}'$*: the component perpendicular to* $\mathbf{M}_{\mathbf{Q}}^{\perp}$ *reverses sign, the parallel component of* $\mathbf{P}$ *is invariant.*

the component of $\mathbf{P}$ perpendicular to $\mathbf{M}_{\mathbf{Q}}^{\perp}$ reverses its sign. This selection rule combined with the $\mathbf{Q}$-dependence provides another simple rule: If $\mathbf{P} \parallel \mathbf{Q}$, the total magnetic scattering will be spin-flip.
Therefore, as exemplified in Moon, Riste, Koehler's seminal paper [14] nuclear and magnetic Bragg peaks can be separated from non-spin-flip and spin-flip scattering respectively b scanning with $\mathbf{P} \parallel \mathbf{Q}$.

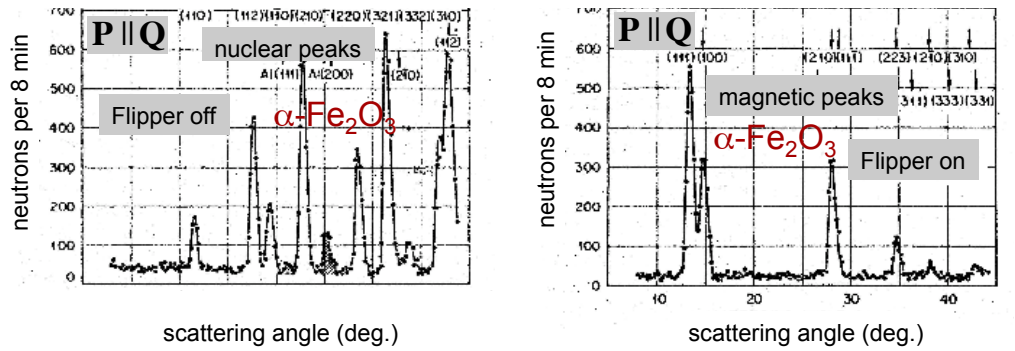

Fig. 16: *Separation of magnetic and nuclear Bragg peaks for powder diffraction from* Fe_2O_3 *by non-spin-flip and spin-flip scattering with* $\mathbf{P} \parallel \mathbf{Q}$*, from Ref.[14].*

3.2 Scattering and polarization analysis, the Blume-Maleyev equations

However, turning from the more simple expressions for the scattering amplitudes to scattering and interference of nuclear and dipolar magnetic interaction potentials, we have to face more complex expressions. As shown by Blume[23] and Maleyev[24], the scattering process can be completely described by two master equations (see Appendix). The first equation gives the scattering cross-section $\sigma_{\mathbf{Q}}$, the second one describes the final polarization $\mathbf{P}'$,

$$\begin{aligned} \sigma_{\mathbf{Q}} &= |N_{\mathbf{Q}}|^2 + |\mathbf{M}_{\mathbf{Q}}^{\perp}|^2 + \mathbf{P}(N_{-\mathbf{Q}}\mathbf{M}_{\mathbf{Q}}^{\perp} + \mathbf{M}_{-\mathbf{Q}}^{\perp}N_{\mathbf{Q}}) + \mathrm{i}\mathbf{P}(\mathbf{M}_{-\mathbf{Q}}^{\perp} \times \mathbf{M}_{\mathbf{Q}}^{\perp}) \\ \mathbf{P}'\sigma_{\mathbf{Q}} &= |N_{\mathbf{Q}}|^2\mathbf{P} + \mathbf{M}_{\mathbf{Q}}^{\perp}(\mathbf{P}\mathbf{M}_{-\mathbf{Q}}^{\perp}) + \mathbf{M}_{-\mathbf{Q}}^{\perp}(\mathbf{P}\mathbf{M}_{\mathbf{Q}}^{\perp}) - \mathbf{P}\mathbf{M}_{\mathbf{Q}}^{\perp}\mathbf{M}_{-\mathbf{Q}}^{\perp} \\ &\quad + \mathbf{M}_{\mathbf{Q}}^{\perp}N_{-\mathbf{Q}} + \mathbf{M}_{-\mathbf{Q}}^{\perp}N_{\mathbf{Q}} + \mathrm{i}\mathbf{M}_{\mathbf{Q}}^{\perp} \times \mathbf{M}_{-\mathbf{Q}}^{\perp} + \mathrm{i}(\mathbf{M}_{\mathbf{Q}}^{\perp}N_{-\mathbf{Q}} - \mathbf{M}_{-\mathbf{Q}}^{\perp}N_{\mathbf{Q}}) \times \mathbf{P} \end{aligned} \tag{17}$$

The notation uses $-\mathbf{Q}$ to denote the complex conjugate. Here, for simplicity only the $\mathbf{Q}$-dependence is specified for Bragg scattering or diffuse scattering. However, in a more general form they apply to inelastic scattering and can be related to van Hove correlation functions (see Appendix).

These equations readily show the different information that can be obtained from an unpolarized with respect to a polarized experiment. While unpolarized neutrons only measure the sum of nuclear and magnetic intensities, for polarized neutrons additional intensity may arise first, due to possible structural-magnetic (NM-terms) interference and second, due to cross products of the magnetic interaction vector $\mathrm{i}\mathbf{M}_{\mathbf{Q}}^{\perp} \times \mathbf{M}_{-\mathbf{Q}}^{\perp}$ describing chiral correlations in non-collinear spin systems. A look at the second equation for the final polarization reveals that we can identify such terms "NM" and "MxM" even with unpolarized neutrons, because they may create final polarization (set $\mathbf{P} = 0$).

3.3 Spherical neutron polarimetry

Another convenient description is given by the standard convention in spherical neutron polarimetry (SNP), or in other words spherical polarization analysis, expressing the final polarization $\mathbf{P}'$ in a tensor equation [25]

$$\mathbf{P}'\sigma \;=\; (|N|^2 + \boldsymbol{\mathcal{R}})\mathbf{P} + \mathbf{P}'' \tag{18}$$

in which the first term $(|N|^2+\boldsymbol{\mathcal{R}})\mathbf{P}$ consists of the scalar nuclear scattering $|N|^2$ and the matrix $\boldsymbol{\mathcal{R}}$ describing the rotation of $\mathbf{P}$, and $\mathbf{P}''$ is the created polarization.
Using the common specific orthogonal setting $\mathbf{x}$ parallel to $\mathbf{Q}$, and $\mathbf{y}$ and $\mathbf{z}$ perpendicular to $\mathbf{Q}$, horizontally and vertically set to the scattering plane respectively, $\boldsymbol{\mathcal{R}}$ and $\mathbf{P}$" are obtained as

$$\begin{aligned}
\boldsymbol{\mathcal{R}} &= \begin{pmatrix} -|M_y|^2 - |M_z|^2 & 2\,Im\,[NM_z] & 2\,Im\,[NM_y] \\ -2\,Im\,[NM_z] & +|M_y|^2 - |M_z|^2 & 2\,Re\,[M_yM_z] \\ -2\,Im\,[NM_y] & 2\,Re\,[M_zM_y] & -|M_y|^2 + |M_z|^2 \end{pmatrix} \\
\mathbf{P}'' &= (-2\,Im\,[M_yM_z]\,,\, 2Re[NM_y]\,,\, 2Re\,[NM_z])
\end{aligned}$$

In general, to detect all elements of the tensor $\boldsymbol{\mathcal{R}}$, one needs spherical neutron polarimetry SNP. Experimentally this can be achieved with a Cryopad device [18] using superconducting material to shield the sample area from magnetic fields. In a MuPaD device, likewise μ-metal is used obtain the zero field condition, which prevents undesired precessions. In particular, SNP is important because it allows to distinguish a rotation from a depolarization of the beam. Depolarization may occur due to an incoherent superposition of intensities with different polarization, this includes spin-incoherent scattering, and more important for determining magnetic structures, intensity from different magnetic domains. See Ref.[25] for detailed examples and analysis.
We may note that SNP does not necessarily require zero field conditions, if the precession can be controlled. Therefore, one can start with precessing polarization $\mathbf{P}$ and analyze the non-precessing polarization $\mathbf{P}'$ along the field. This provides a relatively simple principle, which in contrast to zero-field methods works even for multi-detectors and time-of-flight instruments[26, 27], see also Appendix A.2.

3.4 Uniaxial neutron polarization analysis

Most polarized neutron work is performed on TAS instruments with only uniaxial polarization analysis, sometimes also called longitudinal polarization analysis, which limits the information to the trace of the polarization transfer tensor. Typical applications are like those demonstrated in the experiments by Moon, Riste and Koehler, the separation of magnetic scattering and its directional dependence, and of nuclear coherent and nuclear spin-incoherent scattering.

Half-polarized experiments

Nuclear (or structural) -magnetic (NM) interference and chiral interference can be determined not only by SNP from the off-diagonals of $\boldsymbol{\mathcal{R}}$ but experimentally much simpler in "half-polarized" experiments, by reversing the direction of $\mathbf{P}$.

$$\begin{aligned}
\sigma_{\mathbf{Q}}(\mathbf{P}) - \sigma_{\mathbf{Q}}(-\mathbf{P}) &= 2\mathbf{P}(N_{-\mathbf{Q}}\mathbf{M}^{\perp}_{\mathbf{Q}} + \mathbf{M}^{\perp}_{-\mathbf{Q}}N_{\mathbf{Q}}) + 2\mathrm{i}\mathbf{P}(\mathbf{M}^{\perp}_{-\mathbf{Q}} \times \mathbf{M}^{\perp}_{\mathbf{Q}}) \\
&= -2\,Im\,[M_yM_z]_x\,,\, 2Re[NM_y]\,,\, 2Re\,[NM_z] \text{ for } \mathbf{P} = P_x,\; P_y, \text{and } P_z
\end{aligned}$$

The possible three terms are distinguished by the direction of $\mathbf{P}$ alone and there is no need for polarization analysis. Because of the orientation of $\mathbf{P}$ to M_y and M_z, chirality is seen in spin-flip and nuclear-magnetic interference in non-spinflip mode. NM interference can follow from either accidental coherence, external fields or inherent correlations. Applying magnetic fields in paramagnets, the NM terms measured at Bragg peaks yields a susceptibility for the atomic sites of the crystal. The example of magnetization distribution in iron oxid nanoparticles, see Fig. 14, has been determined with this approach from the nuclear magnetic interference rather than from the magnetic scattering $|\mathbf{M}_{\mathbf{Q}}^{\perp}|^2$.

XYZ-polarization analysis for isotropic samples, paramagnets and powders

Recall that by measuring with $\mathbf{P} \parallel \mathbf{Q}$ and $\mathbf{P} \perp \mathbf{Q}$, one separates and distinguishes nuclear coherent, sin-incoherent and magnetic scattering, It is straightforward to generalize the separation for magnetic powder diffraction for the use of multi-detectors, although in this case it is not possible to set the polarization parallel to all $\mathbf{Q}$ simultaneously. Therefore, one uses the method of **xyz-polarization analysis** [28], and measurements of spin-flip and non-spin-flip intensities are taken with the polarization set into three orthogonal directions, say with z perpendicular to the scattering plane. By the two horizontal polarization settings, we collect the sum of the in-plane and out-of plane magnetic intensities. The following linear combinations eliminate all nuclear scattering contributions and yield the magnetic scattering only[28]. The pre-condition is isotropy, valid for powder samples, and the method is applicable to paramagnets and antiferromagnetic ordered systems (ferromagnets cause depolarization).

$$\frac{d\sigma}{d\Omega}_{pm} = 2\left(\frac{d\sigma}{d\Omega_{\mathrm{x}}}^{SF} + \frac{d\sigma}{d\Omega_{\mathrm{y}}}^{SF} - 2\frac{d\sigma}{d\Omega_{\mathrm{z}}}^{SF}\right) = -2\left(\frac{d\sigma}{d\Omega_{\mathrm{x}}}^{NSF} + \frac{d\sigma}{d\Omega_{\mathrm{y}}}^{NSF} - 2\frac{d\sigma}{d\Omega_{\mathrm{z}}}^{NSF}\right) , \qquad (19)$$

Fig. 17 shows the XYZ-separation results for the magnetic diffuse scattering from a molecular magnet.

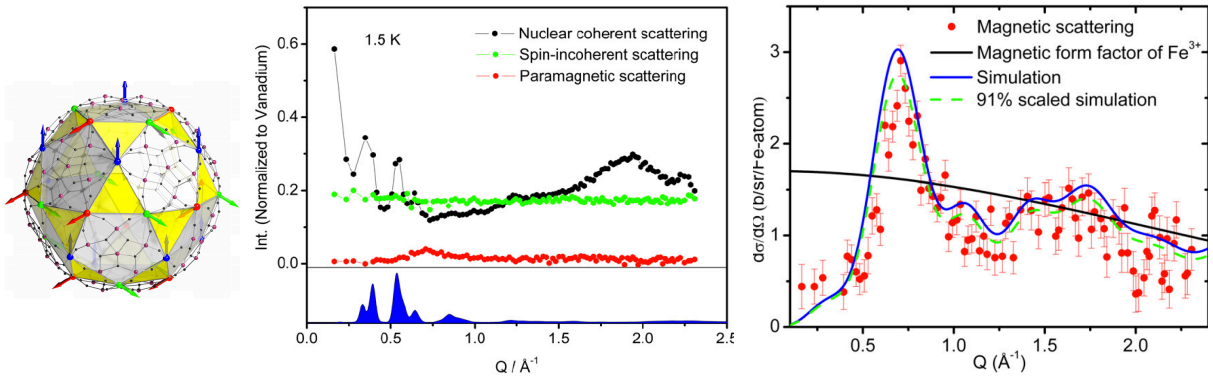

Fig. 17: *$Mo_{72}Fe_{30}X$ molecule (magnetic Fe-ions at vertices, Mo-purple; X: O-black, H, C not shown) and a 3-sublattice non-collinear spin model resulting from AF Heisenberg exchange* (left). *XYZ-separation of weak magnetic intensities* (middle). *Comparison of the magnetic intensity and the spin-model calculation* (right).*[29]*

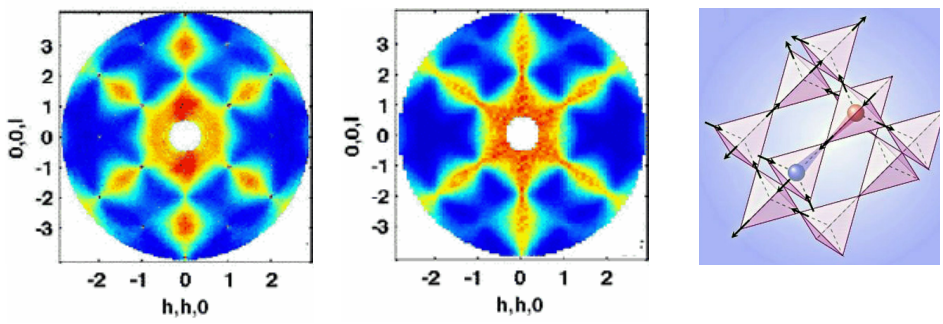

Fig. 18: *Magnetic monopoles evidenced in the diffuse scattering from spin ice, $Ho_2Ti_2O_7$, (*middle*) experimental SF scattering at T = 1.7 K with pinch points at (0,0,2), (1,1,1), and (2,2,2); (*right*) Monte Carlo simulations of the near neighbour model. [31]*

XYZ-polarization analysis for single crystals

For scattering from single crystals all terms in the Blume-Maleyev equations need to be considered. However, there is a new approach, which provides a valid XYZ-polarization analysis for single crystals, making a full separation from the diagonal terms alone by including polarization reversal, see Ref.[30]. The method also applies to inelastic scattering. The premise is the absence of different magnetic domains. Hence, a valid application is the diffuse scattering of homogeneous states in disordered phases, where the efficient use of multi detectors is particularly valuable.

The example on a "spin-ice" system $Ho_2Ti_2O_7$, a cubic pyroclore structure, Fig. 18, shows a measurement of a single polarization element, spin-flip in vertical polarization, which gives essentially the correlations of the in-plane magnetic components. The tetrahedral network and Ising $\langle 111 \rangle$ spin-anisotropy leads to strong frustration for ferro-type exchange. In the ordered state the local spin-correlations can be described for each tetrahedra by a simple rule: two spins are pointing along the $\langle 111 \rangle$ cube diagonals towards the center of the tetrahedra and two spins point outwards. Actually this rule is the perfect analogue to the ice rules in hexagonal ice, describing the hydrogen bonds around the tetrahedral environment of the O ions. Hence Pauling's famous ice model also explains why there should be a residual entropy due to remaining disorder in spin-ice, which is the origin of the broad diffuse scattering at low temperatures. The extraordinary features of this diffuse scattering are so-called pinch-points, the saddle-points in intensity at (111) and (200) positions; on one hand the intensity variation radially, along the modulus of Q, is rather smooth, involving short-range correlations, on the other hand the transverse variation at constant Q is almost discontinuous and singular, which involves many Fourier coefficients and long-range correlations. The explanation is that the ice-topology creates effectively long-range interactions, – any local decision for a specific two-in two-out spin configuration imposes far-reaching constraints for the other tetrahedra –, an effective interaction that can be mapped to Coulomb interaction between monopoles and provides a picture, where the dipole moments in their local sums over four tetrahedral sites can be viewed as two separated monopoles.[31]

A Appendices

A.1 Density matrix formulation

Properties of Pauli spin matrices

$\hat{\boldsymbol{\sigma}} = (\hat{\sigma}_x, \hat{\sigma}_y, \hat{\sigma}_z)$, $\quad \hat{\sigma}_{\rm x} = \begin{pmatrix} 0 & 1 \\ 1 & 0 \end{pmatrix}, \hat{\sigma}_{\rm y} = \begin{pmatrix} 0 & -{\rm i} \\ {\rm i} & 0 \end{pmatrix}, \hat{\sigma}_z = \begin{pmatrix} 1 & 0 \\ 0 & -1 \end{pmatrix}$.
$\hat{\sigma}_\alpha \hat{\sigma}_\beta = \delta_{\alpha\beta} + {\rm i} \sum_\gamma \epsilon_{\alpha\beta\gamma} \hat{\sigma}_\gamma$
$Tr(\hat{\sigma}_\alpha \hat{\sigma}_\beta) = \delta_{\alpha\beta}$
$Tr(\hat{\sigma}_\alpha \hat{\sigma}_\beta \hat{\sigma}_\gamma) = 2{\rm i}\, \epsilon_{\alpha\beta\gamma}$
$Tr(\hat{\sigma}_\alpha \hat{\sigma}_\beta \hat{\sigma}_\gamma \hat{\sigma}_\delta) = 2(\delta_{\alpha\beta}\delta_{\gamma\delta} - \delta_{\alpha\gamma}\delta_{\beta\delta} - \delta_{\alpha\delta}\delta_{\beta\gamma})$

Neutron polarization density matrix

The 2×2 neutron polarization density matrix $\hat{\rm P}$ is a linear combination of the identity matrix and the Pauli spin matrices, $\hat{\rm P} = \frac{1}{2}\left\{\left(\begin{smallmatrix} 1 & 0 \\ 0 & 1 \end{smallmatrix}\right) + \boldsymbol{P}\hat{\boldsymbol{\sigma}}\right\}$, with the polarization vector $\boldsymbol{P} = \langle\hat{\boldsymbol{\sigma}}\rangle$
In the eigenstates of $\hat{\sigma}_z$,
$\hat{\rm P} = \left(\begin{smallmatrix} 1 & 0 \\ 0 & 0 \end{smallmatrix}\right)$ for spin up state $|\uparrow\rangle = |+\rangle$,
$\hat{\rm P} = \left(\begin{smallmatrix} 0 & 0 \\ 0 & 1 \end{smallmatrix}\right)$ for spin down state $|\downarrow\rangle = |-\rangle$,
$\hat{\rm P} = \frac{1}{2}\left(\begin{smallmatrix} 1 & 0 \\ 0 & 1 \end{smallmatrix}\right)$ means unpolarized.
$\boldsymbol{P} = \langle\hat{\boldsymbol{\sigma}}\rangle = Tr(\hat{\rm P}\hat{\boldsymbol{\sigma}}) = \frac{1}{2}\{Tr(\hat{\boldsymbol{\sigma}}) + \boldsymbol{P}Tr(\hat{\boldsymbol{\sigma}}\hat{\boldsymbol{\sigma}})\}$.
$\langle\hat{\rm P}\rangle = Tr(\hat{\rm P}\hat{\rm P}) = \frac{1}{2}(1 + |\boldsymbol{P}|^2)$.
Boundaries for unpolarized and polarized states $\frac{1}{2} \le |\hat{\rm P}| = |\hat{\boldsymbol{\sigma}}| \le 1$ and $0 \le |\boldsymbol{P}| \le 1$.

Polarized neutron scattering cross section

Differential inelastic scattering cross section for polarized neutrons

$$\frac{d^2\sigma}{d\Omega dE'} = \frac{k'}{k} \sum_{\lambda,\sigma} p_\lambda p_\sigma \sum_{\lambda',\sigma'} \langle\lambda,\sigma|\hat{\rm V}^+_{\mathbf{Q}}|\lambda',\sigma'\rangle\langle\lambda',\sigma'|\hat{\rm V}_{\mathbf{Q}}|\lambda,\sigma\rangle \delta(E_\lambda - E_{\lambda'} + \hbar\omega)$$

$$\hat{\rm V}_{\mathbf{Q}} = \hat{b}_{\mathbf{Q}} + \hat{\boldsymbol{\sigma}}\hat{\boldsymbol{\alpha}}_{\mathbf{Q}}, \text{with } \hat{b}_{\mathbf{Q}} = \sum_m b_m e^{-i\mathbf{Q}\cdot\mathbf{R}_m} \text{ and } \hat{\boldsymbol{\alpha}}_{\mathbf{Q}} = \sum_m B_m \hat{\boldsymbol{\sigma}} \hat{\mathbf{I}}_m e^{-i\mathbf{Q}\cdot\mathbf{R}_m} + \frac{\gamma r_0}{2\mu_B}\hat{\boldsymbol{\sigma}}\hat{\mathbf{M}}^\perp_{\mathbf{Q}}$$

$$\sum_{\sigma,\sigma'} p_\sigma \langle\sigma|\hat{\rm V}^+_{\mathbf{Q}}|\sigma'\rangle\langle\sigma'|\hat{\rm V}_{\mathbf{Q}}|\sigma\rangle = \sum_\sigma p_\sigma \langle\sigma|\hat{\rm V}^+_{\mathbf{Q}}\hat{\rm V}_{\mathbf{Q}}\hat{\rm P}|\sigma\rangle = Tr_\sigma(\hat{\rm V}^+_{\mathbf{Q}}\hat{\rm V}_{\mathbf{Q}}\hat{\rm P}) = Tr_\sigma(\hat{\rm P}\hat{\rm V}^+_{\mathbf{Q}}\hat{\rm V}_{\mathbf{Q}})$$

$$Tr_\sigma(\hat{\rm P}\hat{\rm V}^+_{\mathbf{Q}\lambda'\lambda}\hat{\rm V}_{\mathbf{Q}\lambda\lambda'}) = \frac{1}{2}Tr_\sigma\left\{(1 + \mathbf{P}\hat{\boldsymbol{\sigma}})(\hat{b}^+_{\mathbf{Q}\lambda'\lambda} + \hat{\boldsymbol{\alpha}}^+_{\mathbf{Q}\lambda'\lambda}\hat{\boldsymbol{\sigma}})(\hat{b}_{\mathbf{Q}\lambda\lambda'} + \hat{\boldsymbol{\alpha}}_{\mathbf{Q}\lambda\lambda'}\hat{\boldsymbol{\sigma}})\right\}$$
$$= \hat{b}^+_{\mathbf{Q}\lambda'\lambda}\hat{b}_{\mathbf{Q}\lambda\lambda'} + \hat{\boldsymbol{\alpha}}^+_{\mathbf{Q}\lambda'\lambda}\hat{\boldsymbol{\alpha}}_{\mathbf{Q}\lambda\lambda'} + \hat{b}^+_{\mathbf{Q}\lambda'\lambda}(\hat{\boldsymbol{\alpha}}_{\mathbf{Q}\lambda\lambda'}\cdot\mathbf{P}) + (\hat{\boldsymbol{\alpha}}^+_{\mathbf{Q}\lambda'\lambda}\cdot\mathbf{P})\hat{b}_{\mathbf{Q}\lambda\lambda'} + {\rm i}\mathbf{P}\cdot(\hat{\boldsymbol{\alpha}}^+_{\mathbf{Q}\lambda'\lambda}\times\hat{\boldsymbol{\alpha}}_{\mathbf{Q}\lambda\lambda'})$$

$$\frac{d^2\sigma}{d\Omega dE'} = \frac{k'}{k}\left([\hat{b}^+_{\mathbf{Q}}\hat{b}_{\mathbf{Q}}]_\omega + [\hat{\boldsymbol{\alpha}}^+_{\mathbf{Q}}\cdot\hat{\boldsymbol{\alpha}}_{\mathbf{Q}}]_\omega + [\hat{b}^+_{\mathbf{Q}}(\hat{\boldsymbol{\alpha}}^+_{\mathbf{Q}}\cdot\mathbf{P})]_\omega + [(\hat{\boldsymbol{\alpha}}_{\mathbf{Q}}\cdot\mathbf{P})\hat{b}_{\mathbf{Q}}]_\omega + {\rm i}\mathbf{P}\cdot[\hat{\boldsymbol{\alpha}}^+_{\mathbf{Q}}\times\hat{\boldsymbol{\alpha}}_{\mathbf{Q}}]_\omega\right)$$

$$\left[\hat{\rm A}^+_{\mathbf{Q}}\hat{\rm B}_{\mathbf{Q}}\right]_\omega = S_{\rm AB}(\mathbf{Q},\omega) = \frac{1}{2\pi}\int dt\, \exp({\rm i}\omega(t))\langle\hat{\rm A}^+_{\mathbf{Q}}(t)\hat{\rm B}_{\mathbf{Q}}(0)\rangle$$

$$\text{Polarization of the scattered beam} \quad \mathbf{P}' = \langle\hat{\boldsymbol{\sigma}}\rangle = \frac{Tr(\hat{\mathrm{P}}\hat{\mathrm{V}}^{+}_{\mathbf{Q}}\hat{\boldsymbol{\sigma}}\hat{\mathrm{V}}_{\mathbf{Q}})}{Tr(\hat{\mathrm{P}}\hat{\mathrm{V}}^{+}_{\mathbf{Q}}\hat{\mathrm{V}}_{\mathbf{Q}})}$$

$$\begin{aligned}
Tr_\sigma(\hat{\mathrm{P}}\hat{\mathrm{V}}^{+}_{\mathbf{Q}\lambda'\lambda}\hat{\boldsymbol{\sigma}}\hat{\mathrm{V}}_{\mathbf{Q}\lambda\lambda'}) &= \frac{1}{2}Tr_\sigma\left\{(1+\mathbf{P}\hat{\boldsymbol{\sigma}})(\hat{b}^{+}_{\mathbf{Q}\lambda'\lambda}+\hat{\boldsymbol{\alpha}}^{+}_{\mathbf{Q}\lambda'\lambda}\hat{\boldsymbol{\sigma}})\hat{\boldsymbol{\sigma}}(\hat{b}_{\mathbf{Q}\lambda\lambda'}+\hat{\boldsymbol{\alpha}}_{\mathbf{Q}\lambda\lambda'}\hat{\boldsymbol{\sigma}})\right\} \\
\text{(nuclear)} &= \hat{b}^{+}_{\mathbf{Q}\lambda'\lambda}\hat{b}_{\mathbf{Q}\lambda\lambda'}\mathbf{P} \\
\text{(magnetic)} &\quad + \hat{\boldsymbol{\alpha}}^{+}_{\mathbf{Q}\lambda'\lambda}(\hat{\boldsymbol{\alpha}}_{\mathbf{Q}\lambda\lambda'}\cdot\mathbf{P}) + (\hat{\boldsymbol{\alpha}}^{+}_{\mathbf{Q}\lambda'\lambda}\cdot\mathbf{P})\hat{\boldsymbol{\alpha}}_{\mathbf{Q}\lambda\lambda'} - \mathbf{P}(\hat{\boldsymbol{\alpha}}^{+}_{\mathbf{Q}\lambda'\lambda}\hat{\boldsymbol{\alpha}}_{\mathbf{Q}\lambda\lambda'}) \\
\text{(nuclear}-\text{magnetic NM)} &\quad + \hat{b}^{+}_{\mathbf{Q}\lambda'\lambda}\hat{\boldsymbol{\alpha}}_{\mathbf{Q}\lambda\lambda'} + \hat{\boldsymbol{\alpha}}^{+}_{\mathbf{Q}\lambda'\lambda}\hat{b}_{\mathbf{Q}\lambda\lambda'} \\
\text{(chiral)} &\quad - \mathrm{i}\hat{\boldsymbol{\alpha}}^{+}_{\mathbf{Q}\lambda'\lambda}\times\hat{\boldsymbol{\alpha}}_{\mathbf{Q}\lambda\lambda'} \\
\text{(rotation by NM)} &\quad + \mathrm{i}\mathbf{P}\times[\hat{\boldsymbol{\alpha}}^{+}_{\mathbf{Q}\lambda'\lambda}\hat{b}_{\mathbf{Q}\lambda\lambda'} - \hat{b}^{+}_{\mathbf{Q}\lambda'\lambda}\hat{\boldsymbol{\alpha}}_{\mathbf{Q}\lambda\lambda'}]
\end{aligned}$$

$$\begin{aligned}
\mathbf{P}'\frac{d^2\sigma}{d\Omega dE'} &= \frac{k'}{k}(\ \mathbf{P}[\hat{b}^{+}_{\mathbf{Q}}\hat{b}_{\mathbf{Q}}]_\omega + [\hat{\boldsymbol{\alpha}}^{+}_{\mathbf{Q}}(\mathbf{P}\cdot\hat{\boldsymbol{\alpha}}_{\mathbf{Q}})]_\omega + [\hat{\boldsymbol{\alpha}}_{\mathbf{Q}}(\mathbf{P}\cdot\hat{\boldsymbol{\alpha}}^{+}_{\mathbf{Q}})]_\omega - \mathbf{P}[\hat{\boldsymbol{\alpha}}^{+}_{\mathbf{Q}}\cdot\hat{\boldsymbol{\alpha}}_{\mathbf{Q}}]_\omega \\
&\quad +\ [\hat{b}^{+}_{\mathbf{Q}}\hat{\boldsymbol{\alpha}}_{\mathbf{Q}}]_\omega + [\hat{\boldsymbol{\alpha}}^{+}_{\mathbf{Q}}\hat{b}_{\mathbf{Q}}]^{+}_{\omega} + \mathrm{i}\cdot[\hat{\boldsymbol{\alpha}}^{+}_{\mathbf{Q}}\times\hat{\boldsymbol{\alpha}}_{\mathbf{Q}}]_\omega \\
&\quad +\ \mathrm{i}\mathbf{P}\times[\hat{\boldsymbol{\alpha}}^{+}_{\mathbf{Q}}\hat{b}_{\mathbf{Q}} - \hat{b}^{+}_{\mathbf{Q}}\hat{\boldsymbol{\alpha}}_{\mathbf{Q}}]_\omega\ )
\end{aligned}$$

A.2 Precession spherical neutron polarimetry

Although scattering terms of all correlation functions appear on the trace of the polarization tensor, and can be separated from the twelve measurements with spinflip, non-spinflip and field reversal,[30] the off-diagonal terms are of interest in case of magnetic domains. In view of the instrumentation at the new spallation sources, one should note that multi-detector and time-of flight instruments can not apply zero field techniques for SNP, however, a precession technique for SNP has been developed for this purpose and been demonstrated at on the DNS instrument [26, 27]. Most important to note is that by measuring the non-precessing final component, one can readily measure and analyze the polarization of the scattering simultaneously for all $\mathbf{Q}$ and ω.

The principle idea is to start with precessing incident polarization and to analyze the non-precessing final polarized scattering. Therefore, (i) a $\pi/2$ flipper set the polarization into precession mode, (ii) a variation of the field strength before the sample determines the precession angle and the polarization at the sample, (iii) a variation of the field direction before the sample will rotate the precession plane to access all matrix elements; a simulation and an experiment are shown in Fig. 19 and Fig. 20.

One of the early successful examples of spherical polarization analysis solving a complex antiferromagnetic structure is the study of $U_{14}Au_{51}$ by zero-field polarimetry on CryoPad[32]. It is a magnetic structure with zero propagation vector, for which nuclear and magnetic Bragg peaks coincide. We repeated the experiment on DNS with the new precession technique. Fig. 20 illustrates the identification of nuclear and magnetic scattering for the (201) Bragg peak. The crystal is oriented vertically with its b-axis parallel to z. The spins are ordered within the a-b plane with a hexagonal star-like structure. The nuclear scattering is confirmed by a measurement above the Neel temperature at 30K and remains independent of the polarisation. Maxima are found for a rotation of the polarisation from the z to the y direction. For an initial polarisation along x

(which is set parallel to the scattering vector) only spin-flip scattering is observed for the magnetic scattering, as it must be. For all cases, when taking nuclear scattering into account, an effective depolarisation is observed. These results are in excellent agreement with the results obtained with CryoPAD [32].

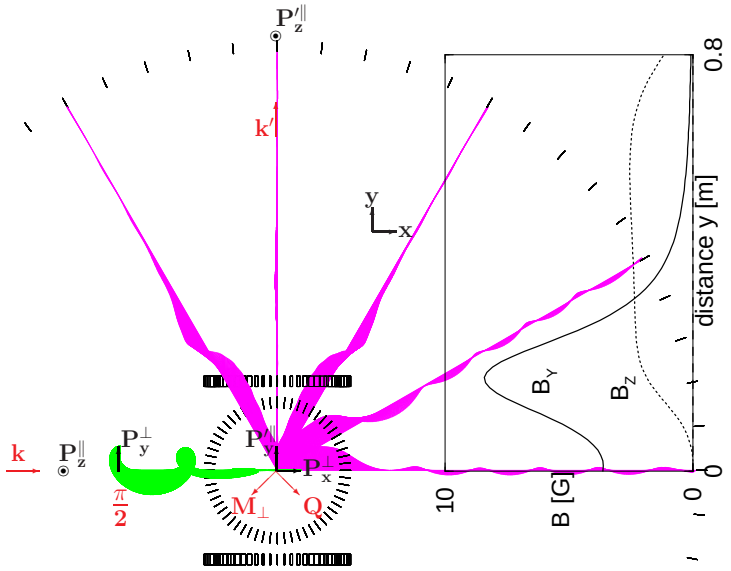

Fig. 19: *Simulation of precessing neutron polarisation analysis for typical parameters of the DNS instrument. Neutrons with wave-vector $\vec{k}$ are (i) polarized in P_z, (ii) undergo a $\pi/2$-flip to P_y, and (iii) precess to the sample to P_x in a field turning the normal vector of the precessing plane from z to y. Scattering is simulated for five different scattering angles, and in each case the final polarization turns up adiabatically from P_y to P_z. The inset shows the field variation for 90^o scattering.*

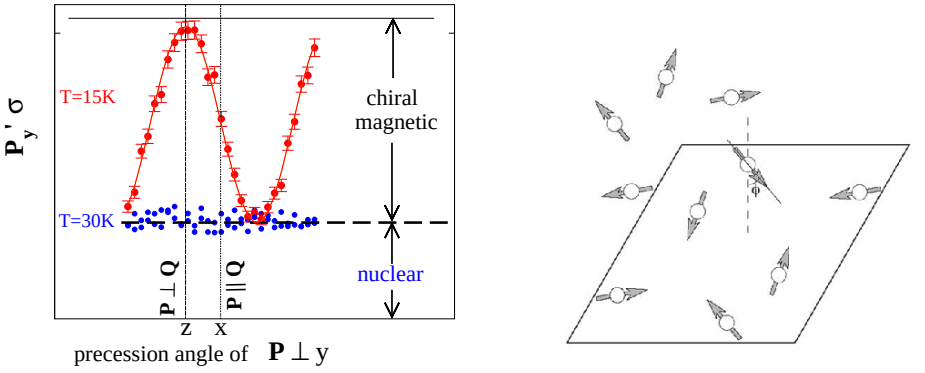

Fig. 20: *Spherical polarisation analysis on the (201) Bragg peak of $U_{14}Au_{51}$. The initial polarisation precesses perpendicular to the applied field in y-direction. At 30 K there is only a nuclear Bragg component which continues to precess after the scattering event. At lower temperatures, T=15 K, there is an additional magnetic contribution for which the neutron polarisation changes from $\mathbf{P} \parallel z$ to $\mathbf{P}' \parallel y$.*

For interested readers in polarized neutron studies, I like to recommend particularly the lectures of Andrey Zheludev [33], giving a more thorough discussion and a variety of examples for applications, as well as the lectures and publications of Otto Schärpf [21], which can be found on his homepage.

References

[1] Alvarez, L. W., F. A. Bloch, Quantitative determination of the neutron magnetic moment in absolute nuclear magnetons, Phys. Rev. **57**, 111 (1940).

[2] First determination of the negative sign of γ_n, P.N. Powers, The magnetic scattering of neutrons, Phys. Rev. **54**, 827 (1938).

[3] Charles M. Sommerfield, Phys. Rev. **107**, 328 (1957).

[4] Julian Schwinger, Phys. Rev. **73**, 416 (1948).

[5] G. P. Felcher, S. Adenwalla, V. O. De Haan and A. A. Vav Well, Nature **377**, 409 (1995).

[6] O. Schärpf, in *Neutron Spin Echo* Lecture Notes in Physics **128**, Ed. F. Mezei, Springer, pp. 27-52 (1980).

[7] F. Klein, *The mathematical theory of the top*, Princeton 1897; see also H. Goldstein, *Klassische Mechanik*, Akademische Verlagsges. Frankfurt am Main (1974).

[8] O. Schärpf, J. Physics E: Sci. Instrum. **8**, 268 (1975); F. Mezei, Commun. Phys. **1**, 81 (1976); P. Böni, J. Neutron Research **5**, 63 (1996).

[9] http://www.swissneutronics.ch/products/coatings.html

[10] E. Babcock *et al.*, www.jcns.info/He3_SEOP.

[11] M. T. Rekveldt, T. Keller and R. Golub, Europhys. Lett. **54**, 342 (2001).

[12] J. Repper *et al.* JCPDS-International Centre for Diffraction Data (2009) ISSN 1097-0002.

[13] P.G. Niklowitz *et al.*, Phys. Rev. Lett. **104**, 106406 (2010).

[14] R.M. Moon, T. Riste, W.C. Koehler, Phys. Rev. **181**, 920 (1969).

[15] W. Schweika and P. Böni, Physica B **297**, 155 (2001).

[16] J. R. Stewart *et al*, J. Appl. Cryst. **42**, 69 (2009).

[17] O. Schärpf, Physica B **182**, 376 (1992).

[18] F. Tasset *et al.*, Physica B **267** (1-4) 69-74 (1999).

[19] G.L. Squires, *Introduction to the theory of thermal neutron scattering*, Cambridge University Press, Cambridge (1978).

[20] A. C. Genix *et. al.* Macromolecules **39**, 3947 (2006).

[21] O. Schärpf, *The spin of the neutron as a measuring probe*, Chapter 11, http://82.135.31.182/neutronpol.pdf

[22] S. Disch *et al.*, New Journal of Physics **14**, 013025 (2012).

[23] M. Blume, Phys. Rev. **130**, 1670 (1963).

[24] S. V. Maleyev, V. G. Baryakhtar P. A. and Suris, Fiz. Tv. Tela **4**, 3461 (1962); Soviet Phys. Solid State **4**, 2533 (1963).

[25] P. J. Brown, J. B. Forsyth, and F. Tasset, Proc. Roy. Soc. London A **442**, 147 (1993); P.J. Brown, *Polarimatric Neutron Scattering*, in lecture notes on *Polarized Neutron Scattering* (Eds. Th. Brückel and W. Schweika), Schriften des Forschungszentrums Jülich, Series Matter and Materials Vol.**12**, Forschungszentrums Jülich (2002).

[26] W. Schweika, Physica B **335** (1-4), 157 (2003).

[27] W. Schweika, S. Easton, and K.-U. Neumann, Neutron News **16**, 14 (2005).

[28] O. Schärpf, H. Capellmann, Phys. Stat. Sol. (a) **135**, 359 (1993).

[29] Z. Fu *al.*, New Journal of Physics **12**, 083044 (2010).

[30] W. Schweika, J. Phys. Conf. Ser. **211**, 012026 (2010).

[31] T. Fennell *et al.* Science **326**, 415 (2009).

[32] P. J. Brown, J. Crangle, K.-U. Neumann, J. G. Smith, and K. R. A. Ziebeck, J. Phys.: Cond. Mat. **9**, 4729 (1997).

[33] www.neutron.ethz.ch/education/Lectures/neutronspring.